

Communication

# Bottom-Up Synthesis of Porous NiMo Alloy for Hydrogen Evolution Reaction

Kailong Hu <sup>1</sup>, Samuel Jeong <sup>1</sup>, Mitsuru Wakisaka <sup>2,3</sup>, Jun-ichi Fujita <sup>1</sup> and Yoshikazu Ito <sup>1,2,\*</sup>

<sup>1</sup> Institute of Applied Physics, Graduate School of Pure and Applied Sciences, University of Tsukuba, Tsukuba, Ibaraki 305-8573, Japan

<sup>2</sup> PRESTO, Japan Science and Technology Agency, Saitama 332-0012, Japan

<sup>3</sup> Graduate School of Engineering, Toyama Prefectural University, 5180 Kurokawa, Imizu, Toyama 939-0398, Japan

\* Correspondence: ito.yoshikazu.ga@u.tsukuba.ac.jp; Tel.: +81-29-853-5247

**Abstract:** Bottom-up synthesis of porous NiMo alloy reduced by NiMoO<sub>4</sub> nanofibers was systematically investigated to fabricate non-noble metal porous electrodes for hydrogen production. The different annealing temperatures of NiMoO<sub>4</sub> nanofibers under hydrogen atmosphere reveal that the 950 °C annealing temperature is a key to produce bicontinuous and monolithic porous NiMo alloy without oxide phases. The porous NiMo alloy as cathodes in electrical water splitting demonstrates not only almost identical catalytic activity with commercial Pt/C, but also superb stability for 12 days.

**Keywords:** nanoporous; NiMo; non-noble metal catalyst; hydrogen evolution

## 1. Introduction

Nanoporous metals are key materials for energy engineering fields because of high conductivity, bi-continuous open porous structures with tunable porosity, large surface area, high catalytic activities and high mechanical strength [1, 2]. Recently, nanoporous non-precious metals have been focused as electrodes and catalysts such as supercapacitor [3, 4], Li-air battery [5, 6], fuel cell and electrolysis of water [7, 8], showing great potentials as precious metal-free electrodes. The fabrication process of nanoporous metal employs a dealloying method [1] that the solid solution alloy of precious metal and non-precious metal was electrochemically corroded in acidic electrolytes. However, in this method, the alloy combinations in the dealloying method is very limited and the non-precious metal of Ni, Fe and Cu is usually the one to be removed from the alloy, forming precious metal-based nanoporous structures. Therefore, the desirable design of non-precious metal has been explored to expand their applications.

Nanoporous non-precious metal have been synthesized by bottom-up approaches such as nanoparticle-sintering [9, 10] and reduction of metal oxides [11, 12]. Especially, the reduction of metal oxide is a powerful method to prepare nanoporous non-precious metal. One of attractive porous metals is NiMo alloy which is known as the best hydrogen evolution electrode catalyst [13, 14] for cost-effective and highly efficient hydrogen production in water electrolysis. Although different kind of NiMo alloy porous morphologies were investigated as HER catalysts including Ni<sub>4</sub>Mo [15], NiMo nanopowder [16], NiMo nanowire [17], the performances show the HER performance is not very enhanced due to the absence of bi-continuous and monolithic porous structures. Indeed, the Ni foam supported Ni<sub>4</sub>Mo nanoparticles and the three-dimensional NiMo nanowires significantly improved their HER activities. This means that bi-continuous and monolithic 3D electrode catalysts bring high reaction kinetics. Therefore, NiMo alloy with bicontinuous open porous 3D structure can be a central electrode catalyst for electrical water splitting combined with renewable energy such as wind, water and solar energies to produce eco-friendly hydrogen production without any carbon emission.

In this study, we have systematically investigated porous NiMo alloy with different annealing temperatures from 400 to 950°C to understand the formation of porous structures by reduction under

hydrogen atmosphere. Moreover, the electrochemical performances of resulting porous NiMo alloy samples were tested in 1 M KOH electrolyte with the comparison of the best catalyst of platinum (Pt). The durability test in 1 M KOH electrolyte was further carried out by cyclic voltammetry and chronoamperometry measurements.

## 2. Materials and Methods

**Preparation of NiMoO<sub>4</sub> nanofibers.** NiMoO<sub>4</sub> nanofibers, synthesized by a standard hydrothermal method [18, 19], were used as precursors to obtain 3D porous NiMo alloy through a reductive annealing system. 2.5 mmol NiCl<sub>2</sub>·6H<sub>2</sub>O (wako, 98% purity) and 2.5 mmol Na<sub>2</sub>MoO<sub>4</sub>·2H<sub>2</sub>O (wako, 99% purity) were dissolved in 30 ml deionized water, and then was transferred into a 50 ml Teflon coated stainless autoclave, which was kept at 150°C for 12 h. After the autoclave cooling down to room temperature, the as-prepared NiMoO<sub>4</sub> nanofibers were washed by deionized water several times with a centrifuge, and kept in deionized water.

**Preparation of porous NiMo alloy.** The NiMoO<sub>4</sub> nanofiber solution was dropped on Cu sheets, and dried naturally for one day. The dried NiMoO<sub>4</sub> was put into the center of a quartz tube ( $\phi 30 \times \phi 27 \times 1000$  mm) furnace. The NiMoO<sub>4</sub> was reduced at various temperatures from 400–950°C for 20 min under the mixed atmosphere of hydrogen (100 sccm) and argon (200 sccm) to reduce oxides for porous structure formation. After the annealing, the resulting reduced samples were removed from the Cu sheets for measurements.

**Imaging and spectroscopic characterization.** The morphology and microstructure of 3D NiMo alloy were characterized by a scanning electron microscope (SEM, JEOL JSM-4300). The X-ray diffraction (XRD) was carried out using a RIGAKU SmartLab 9MTP diffractometer with a 9.0 kW rotating anode generator (Cu K $\alpha$ 1 radiation;  $\lambda = 1.5406$  Å). The X-ray photoelectron spectroscopy (XPS, AXIS ultra DLD, Shimadzu) with Al K $\alpha$  and X-ray monochromator was utilized for surface chemical compositions analysis.

**Electrochemical characterizations.** Hydrodynamic voltammetry for HER and electrochemical impedance spectroscopy (EIS) were conducted using an electrochemical workstation (Biologic, VSP-300) equipped with a rotation disk electrode (RDE, 5 mm diameter grassy carbon, HOKUTO DENKO corp.). A graphite plate, an Ag/AgCl electrode (HOKUTO DENKO corp.) and the porous NiMo samples (5 mg) dispersed on the grassy carbon served as the counter electrode, the reference electrode and the working electrode, respectively. The Ag/AgCl electrode was checked before use. All potentials were calculated with respect to RHE using the equation:  $E(\text{RHE}) = E(\text{Ag/AgCl}) + 0.0591 \times \text{pH} + 0.1976$ . The cyclic voltammetry (CV) measurements after several cycles were recorded from -250 mV to +100 mV (v.s. RHE) at a sweep rate of 10 mV/s in 1 M KOH electrolyte deaerated with Ar (99.999%) with disk rotation speed of 1600 rpm to remove generated hydrogen bubbles. The electrode potential in the hydrodynamic voltammogram was automatically iR-compensated with the Ohmic resistance measured at +200 mV (v.s. RHE). The EIS measurement was carried out at -200 mV (v.s. RHE) with an amplitude of 50 mV. The durability of the electrodes was tested by potential cycling between -250 mV to +100 mV (v.s. RHE) at 10 mV/s.

## 3. Results and Discussion

The fabrication process of 3D porous NiMo alloy, illustrated in **Figure 1**, was divided into two main procedures. Firstly, the NiMoO<sub>4</sub> nanofibers, the precursor of porous NiMo, were synthesized through a standard hydrothermal method at 150°C for 12 hours. Secondly, the resulting NiMoO<sub>4</sub> nanofibers dropped on Cu sheets and inserted into a quartz tube furnace were annealed at 400-950°C for 20 min under the mixed gases of hydrogen and argon to reduce the oxidized precursor. After the furnace cooling down to room temperature, the annealed NiMoO<sub>4</sub> samples were peeled off from the Cu sheets for characterizations and measurements. Moreover, the sheet area easily reached to 2 cm<sup>2</sup> (**Figure 1**) when the area of Cu sheet was tuned.

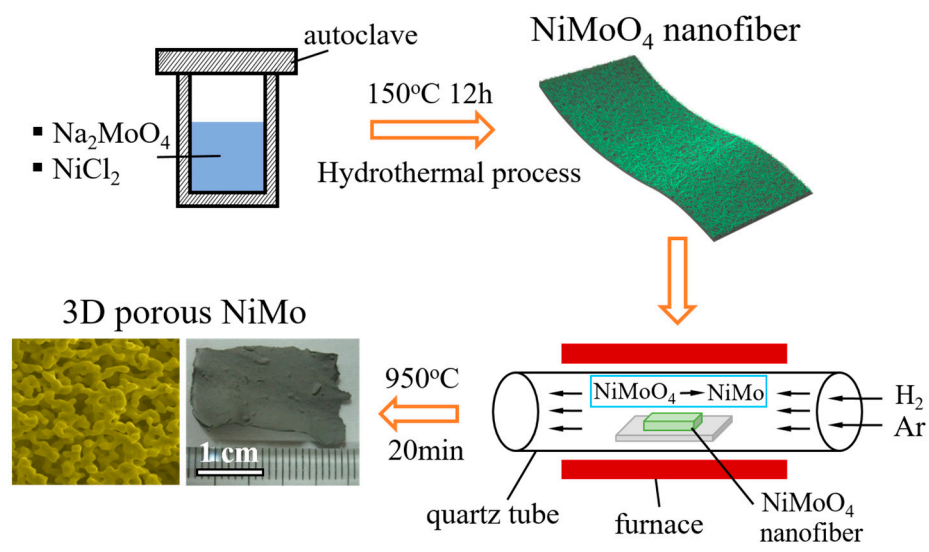


**Figure 1.** Schematic illustration of the synthesis process of 3D porous NiMo alloy.

The morphologies of annealed  $\text{NiMoO}_4$  samples were investigated to reveal the formation process of porous structures with scanning electron microscope (SEM) measurements. The nanofiber structure was kept at low temperatures of  $0\text{--}500^\circ\text{C}$  (**Figure 2a-c**), and some nanoparticles were generated on the surface of nanofibers at  $500^\circ\text{C}$  due to the reduction of  $\text{NiMoO}_4$  nanofibers (inset of **Figure 2c**). When the temperature reached to  $600^\circ\text{C}$ , the generated nanoparticles started to fuse and reconstruct each other to be energetically stable due to the high geometric potential at the nanoparticle state (**Figure 2d**). The pristine nanofiber structures were totally disappeared at  $700^\circ\text{C}$  and the ligaments in the porous structures were gradually formed with pore size less than 100 nm (**Figure 2e**). The 3D open porous structures were developed and the porous structures became bicontinuous and interconnected above  $800^\circ\text{C}$  (**Figure 2f**). The porous structures were well developed and the pore size increased from tens of nanometers to a few hundred nanometers with the temperature ranging from 800 to  $950^\circ\text{C}$  (**Figure 2g-h**). The view of cross-section of sample annealed at  $950^\circ\text{C}$  showed the open and bicontinuous structures were well preserved in the inside of sample sheets (**Figure 2i**).

The crystal structures of annealed  $\text{NiMoO}_4$  samples were studied by X-ray diffraction (XRD) measurements (**Figure 3a**). The pristine  $\text{NiMoO}_4$  nanofibers showed amorphous features and they were not completely assigned well. The sample annealed at  $400^\circ\text{C}$  also showed same characteristic peaks with the pristine  $\text{NiMoO}_4$  nanofibers. This means the  $400^\circ\text{C}$  annealing does not affect the reduction of the oxidized state. When the annealing temperature ranges between  $500\text{--}600^\circ\text{C}$ , the obtained peaks were well assigned to  $\text{NiMoO}_4$  (JCPDS #086-0361). This can be explained with the crystallization of  $\text{NiMoO}_4$  at  $500\text{--}600^\circ\text{C}$ . At  $700^\circ\text{C}$ , some  $\text{NiMoO}_4$  were reduced and decomposed under the reductive atmosphere, partly forming  $\text{NiO}$  (JCPDS #71-1179),  $\text{MoO}_2$  (JCPDS #04-0809) and  $\text{MoO}_3$  (JCPDS #74-7911). Above  $800^\circ\text{C}$ , the composition of  $\text{NiMo}$  (JCPDS #48-1745),  $\text{Ni}_4\text{Mo}$  (JCPDS #65-5480), and pure  $\text{Mo}$  (JCPDS #04-0809) were gradually generated and oxidized species of  $\text{NiO}$  and  $\text{MoO}_2$  were gradually reduced. The  $\text{Ni(OH)}_2$  (JCPDS #14-0117) was created from pure  $\text{Ni}$  when it exposed into air for XRD measurements. It is worthy noted that the reduction of  $\text{NiMoO}_4$  requires  $800^\circ\text{C}$  and reduction of  $\text{MoO}_2$  requires  $950^\circ\text{C}$ . Thus, the sample annealed at  $950^\circ\text{C}$  only obtains  $\text{NiMo}$  with certain amount of  $\text{Ni}_4\text{Mo}$  alloys.

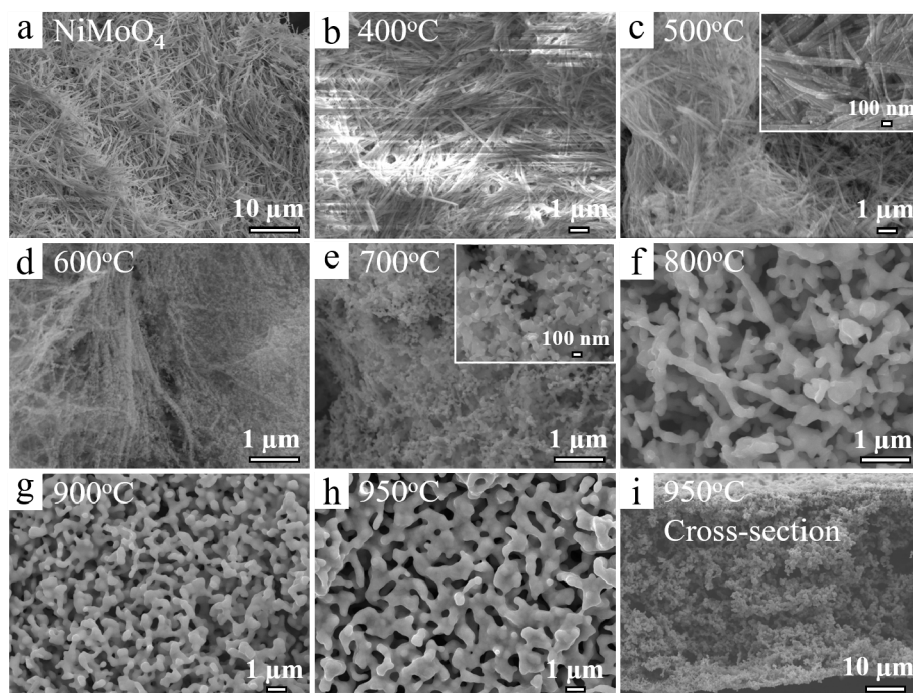


**Figure 2.** SEM images of (a) pristine NiMoO<sub>4</sub> nanofiber, (b-i) temperature effect of 3D porous structure formation on samples annealed at 400°C-950°C. The insets in (c) and (e) show high resolution SEM images.

The surface chemical compositions of porous NiMo and Ni<sub>4</sub>Mo alloy samples annealed at 900°C and 950°C were tested by X-ray photoelectron spectroscopy (XPS) measurements. The high-resolution Ni 2p spectrum of the sample annealed at 900°C reveals that the main peaks are assigned to Ni (852.6 eV, 869.6 eV) and NiO (855.9 eV, 873.6 eV), while the NiO peaks of the sample annealed at 950°C are negligibly small (**Figure 3b, 3d**). These results further indicate that Ni oxides were completely reduced at 950°C. The high-resolution Mo 3d spectrum of samples annealed at 900°C were deconvoluted into six distinct peaks at 227.4 eV, 230.6 eV, 228.5 eV, 231.6 eV, 232.1 eV and 235.2 eV, assigning to NiMo, Ni<sub>4</sub>Mo, Mo<sup>4+</sup> and Mo<sup>6+</sup>, showing alloy and oxidized surface state with mixtures of NiMo and Mo oxides (**Figure 3c**). The sample annealed at 950°C presents major NiMo with negligible Ni<sub>4</sub>Mo and Mo oxides on the surface, further confirming the complete reduction of Mo<sup>4+</sup> and Mo<sup>6+</sup> at 950°C (**Figure 3e**). These XPS results are good agreements with the XRD results. Considering XRD and XPS results during the reduction process, the following sequential transformations are proposed: (1) the reduction of NiMoO<sub>4</sub> to partly-reduced NiMoO<sub>4</sub> nanoparticles, (2) the reconstruction and fusion of the further-reduced NiMoO<sub>4</sub> nanoparticles to decrease the surface energy and (3) the complete reduction of NiMoO<sub>4</sub> nanoparticles for the formation of ligaments into porous NiMo structures, developing 3D porous NiMo alloy.

The samples with different annealing temperatures of 800°C, 900°C and 950°C (abbreviated as NiMo-800°C, NiMo-900°C and NiMo-950°C) with the comparison of commercial 10wt% Pt/C and the pristine NiMoO<sub>4</sub> nanofibers were tested in 1 M KOH solution to investigate the catalytic HER activities (**Figure 4a**). The polarization curve of NiMo-950°C exhibits a Pt-like HER activity, reaching a current density of 10 mA/cm<sup>2</sup> at an overpotential of 18 mV, which is only 2 mV larger than the value achieved by 10wt% Pt/C. The NiMo-900°C and NiMo-800°C reveal a gradual decline trend of HER catalytic activity, which achieve 10 mA/cm<sup>2</sup> at an overpotential of 66 mV and 182 mV. This decline indicates that the existence of Mo oxides and Ni oxides dramatically interferes HER processes, and the HER activity can be greatly enhanced only with the complete reduction of the oxides at 950°C. Indeed, the fully oxidized NiMoO<sub>4</sub> nanofiber exhibits no HER catalytic activity. The Tafel plots estimated from the polarization curves (**Figure 4b**) show that the NiMo-950°C achieves a Tafel slope of 36 mV/decade and 10wt% Pt/C (loading amount: 0.26 mg/cm<sup>2</sup>) exhibits 30 mV/decade. Therefore, the Heyrovsky desorption process ( $\text{H}_2\text{O} + \text{e}^- + \text{H}^* \rightarrow \text{H}_2 + \text{OH}^-$ ), where H<sup>\*</sup> represents adsorbed H



atom on catalytic site \*) could be the rate determining step for the NiMo-950°C in 1 M KOH electrolyte [20]. The Tafel slopes of NiMo-900°C and NiMo-800°C are 72 mV/dec and 147 mV/dec, indicating the mixed Volmer-Heyrovsky process ( $\text{H}_2\text{O} + \text{e}^- + \text{H}^* \rightarrow \text{H}_2 + \text{OH}^-$  and  $\text{H}_2\text{O} + \text{e}^- \rightarrow \text{H}^* + \text{OH}^-$ ) are the corresponding rate determining steps [21, 22]. The EIS measurements were further carried out to measure the charge-transfer resistances ( $R_{\text{ct}}$ ) of the porous NiMo alloys at an overpotential of 200 mV v.s. RHE (Figure 4c). The internal resistances of NiMo-800°C, NiMo-900°C and NiMo-950°C are almost the same value of 5  $\Omega$ . The NiMo-950°C exhibits quite low  $R_{\text{ct}}$  value of 7.9  $\Omega$ , which far lower than the 19.8  $\Omega$  for NiMo-900°C and the 26.5  $\Omega$  for NiMo-800°C, confirming more efficient reaction kinetics of the NiMo-950°C sample.

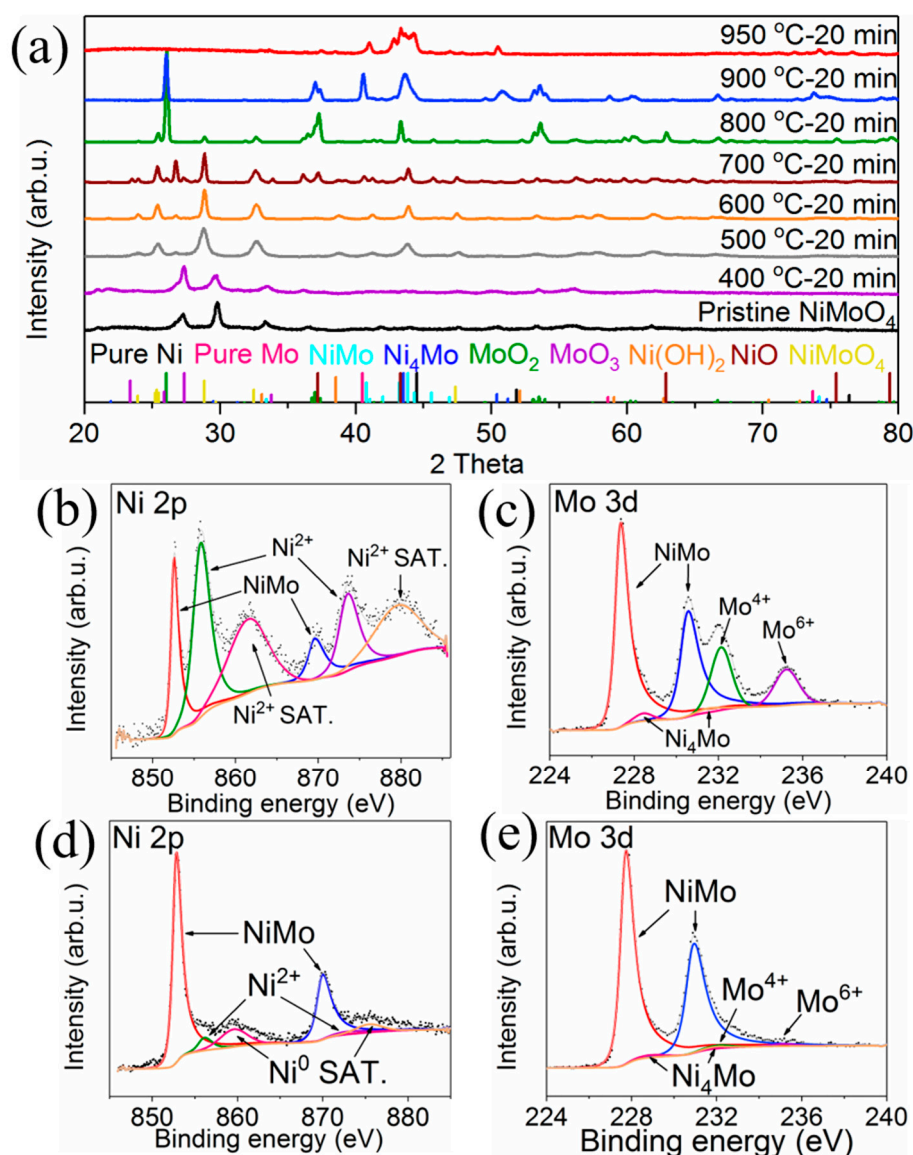


**Figure 3.** (a) XRD patterns of pristine NiMoO<sub>4</sub> nanofibers and reduced samples at different annealing temperatures. High-resolution XPS spectra of nickel 2p and molybdenum 3d spectra on porous NiMo samples annealed at 900°C for 20 min (b-c) and 950°C for 20 min (d-e).

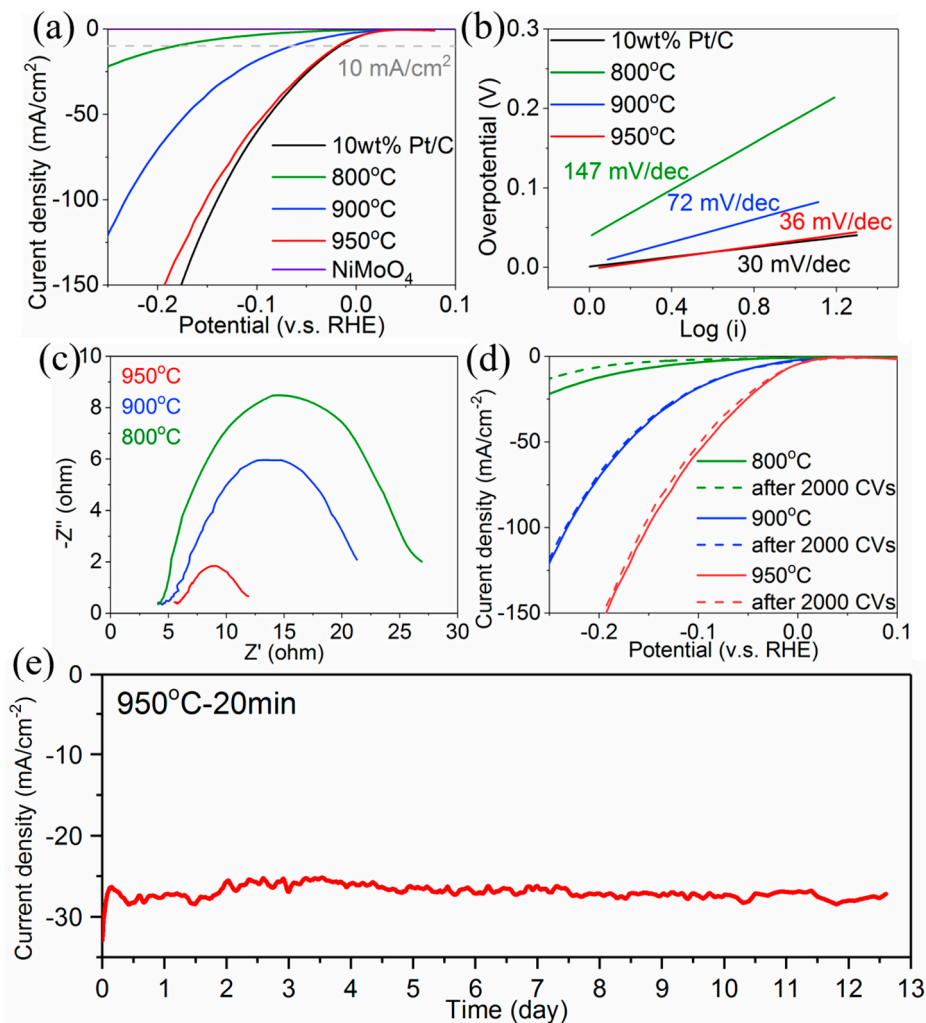


**Figure 4.** (a) The HER polarization curves of porous NiMo samples annealed at 800°C, 900°C, 950°C, pristine NiMoO<sub>4</sub> nanofibers and Pt/C. (b) Corresponding Tafel plots. (c) Electrochemical impedance spectroscopy of porous NiMo samples annealed at 800°C, 900°C and 950°C at overpotential of 200 mV v.s. RHE. (d) Polarization curves of porous NiMo samples annealed at 800°C, 900°C and 950°C before and after 2000 CV cycles. (e) Durability test of porous NiMo annealed at 950°C at overpotential of 200 mV by chronoamperometry.

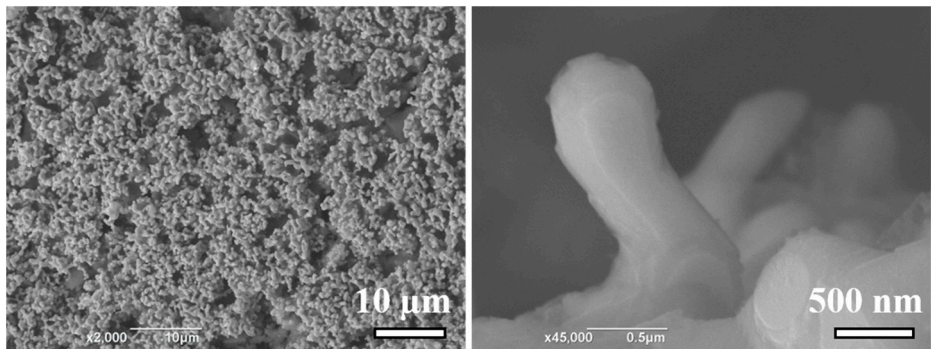


**Figure 5.** SEM images of porous NiMo samples annealed at 950°C after 2000 CV cycles.

The long-term durability is an important criterion for HER cathodes. The CV and chronoamperometry (CA) measurements were utilized to investigate the stability of porous NiMo alloy in 1 M KOH electrolyte. The polarization curves of NiMo-900°C and NiMo-950°C after 2000 cycles exhibit extremely high durability (**Figure 4d**). The overpotential of NiMo-950°C at 100 mA/cm<sup>2</sup> only increases by 5 mV (150 to 155 mV) after the 2000 CV cycles. During the CA measurement (**Figure**

4e), the NiMo-950°C sample (loading amount: 1 mg) keeps original performances of 27 mA/cm<sup>2</sup> for 12.5 days at overpotential of 200 mV. A rotating disk electrode was not used for the CA test, resulting in some bubbles blocked the surface and a slight decrease of the current density. To understand the superb HER performances and chemical stability, the SEM images of the NiMo-950°C sample after 2000 CV cycles were investigated. The bicontinuous porous structure was well preserved in 1 M KOH electrolyte (Figure 5). Thus, chemically stable and well-crystalized porous NiMo-950°C alloy electrode plays an important role of outstanding HER performances.

#### 4. Conclusions

We have demonstrated the formation of porous NiMo alloy with systematic annealing temperatures from 400-950°C. Whereas the formation of porous structures requires 800°C, the complete reduction of Mo oxides species requires 950°C annealing temperature. The completely reduced porous NiMo alloys can be employed as cathodes for electrical water splitting without losing their catalytic abilities in 1 M KOH electrolyte. Such non-noble porous metal alloys could be good replacements of noble metal such as Pt, which has been one of undue barrier to sustaining worldwide use due to high price and low world supply. Therefore, the development and study of non-noble porous metals as low-cost, earth-abundant HER catalysts offer hopeful alternatives to Pt-based catalysts to achieve hydrogen societies.

**Acknowledgments:** We thank Ms. Kazuyo Omura at the Institute for Material Research in Tohoku University for XPS measurements. This work was sponsored by JST-PRESTO "Creation of Innovative Core Technology for Manufacture and Use of Energy Carriers from Renewable Energy" (JPMJPR1541, JPMJPR1444); JSPS KAKENHI Grant Number JP15H05473, JP23246063, JP15H02195, JP15K13717; World Premier International Research Center Initiative (WPI), MEXT, Japan; Japanese Government (MONBUKAGAKUSHO: MEXT) Scholarship.

**Author Contributions:** Hu Kailong, Samuel Jeong and Yoshikazu Ito fabricated samples and conducted SEM characterizations. Yoshikazu Ito and Hu Kailong performed electrochemical tests. Hu Kailong, Mitsuru Wakisaka, Jun-ichi Fujita and Yoshikazu Ito conducted data analysis and data interpretation. Hu Kailong and Yoshikazu Ito wrote the paper.

**Conflicts of Interest:** The authors declare no conflict of interest.

#### References

- Ding, Y.; Chen, M.W. Nanoporous metals for catalytic and optical applications. *MRS Bull.* **2009**, *34*, 569-576, 10.1557/mrs2009.156.
- Weissmüller, J.; Newman, R.C.; Jin, H.J.; Hodge, A.M.; Kysar, J.W. Nanoporous metals by alloy corrosion: formation and mechanical properties. *MRS Bull.* **2009**, *34*, 577-586, 10.1557/mrs2009.157.
- Qiu, H.J.; Ito, Y.; Chen, M.W. Hierarchical nanoporous nickel alloy as three-dimensional electrodes for high-efficiency energy storage. *Scripta Materialia* **2014**, *89*, 69-72, 10.1016/j.scriptamat.2014.06.031.
- Qiu, H.J.; Kang, J.L.; Liu, P.; Hirata, A.; Fujita, T.; Chen, M.W. Fabrication of large-scale nanoporous nickel with a tunable pore size for energy storage. *J. Power Sources* **2014**, *247*, 896-905, 10.1016/j.jpowsour.2013.08.070.
- Guo, X.W.; Han, J.H.; Liu, P.; Ito, Y.; Hirata, A.; Chen, M.W. Graphene@Nanoporous Nickel Cathode for Li-O<sub>2</sub> Batteries. *ChemNanoMat* **2016**, *2*, 176-181, 10.1002/cnma.201500214.
- Guo, X.W.; Liu, P.; Han, J.H.; Ito, Y.; Hirata, A.; Fujita, T.; Chen, M.W. 3D Nanoporous Nitrogen-Doped Graphene with Encapsulated RuO<sub>2</sub> Nanoparticles for Li-O<sub>2</sub> Batteries. *Adv. Mater.* **2015**, *27*, 6137-6143, 10.1002/adma.201503182.
- Linic, S.; Christopher, P.; Ingram, D.B. Plasmonic-metal nanostructures for efficient conversion of solar to chemical energy. *Nature Mater.* **2011**, *10*, 911-921, 10.1038/nmat3151.
- Artero, V.; Kerlidou, M.C.; Fontecave, M. Splitting Water with Cobalt. *Angew. Chem. Int. Ed. Engl.* **2011**, *50*, 7238-7266, 10.1002/anie.201007987.
- Ito, Y.; Izumi, M.; Hojo, D.; Wakisaka, M.; Aida, T.; Adschiri, T. One-step Nanoporous Structure Formation Using NiO Nanoparticles: Pore Size Control and Pore Size Dependence of Hydrogen Evolution Reaction. *Chem. Lett.* **2017**, *46*, 267-270, 10.1246/cl.161017.

9. Hansen, T.W.; DeLaRiva, A.T.; Challa, S.R.; Datye, A.K. Sintering of Catalytic Nanoparticles: Particle Migration or Ostwald Ripening? *Acc. Chem. Res.* **2013**, *46*, 1720-1730, 10.1021/ar3002427.
10. Zhang, J.; Wang, T.; Liu, P.; Liao, Z.Q.; Liu, S.H.; Zhuang, X.D.; Chen, M.W.; Zschech, E.; Feng, X.L. Efficient hydrogen production on MoNi<sub>4</sub> electrocatalysts with fast water dissociation kinetics. *Nat. Commun.* **2017**, *8*, 15437, 10.1038/ncomms15437.
11. Chen, Y.Y.; Zhang, Y.; Zhang, X.; Tang, T.; Luo, H.; Niu, S.; Dai, Z.H.; Wan, L.J.; Hu, J.S. Self-Templated Fabrication of MoNi<sub>4</sub>/MoO<sub>3-x</sub> Nanorod Arrays with Dual Active Components for Highly Efficient Hydrogen Evolution. *Adv. Mater.* **2017**, 1703311, 10.1002/adma.201703311.
12. McCrory, C.C.; Jung, S.; Ferrer, I.M.; Chatman, S.M.; Peters, J.C.; Jaramillo, T.F. Benchmarking hydrogen evolving reaction and oxygen evolving reaction electrocatalysts for solar water splitting devices. *J. Am. Chem. Soc.* **2015**, *137*, 4347-4357, 10.1021/ja510442p.
13. McCrory, C.C.; Jung, S.; Peters, J.C.; Jaramillo, T.F. Benchmarking heterogeneous electrocatalysts for the oxygen evolution reaction. *J. Am. Chem. Soc.* **2013**, *135*, 16977-16987, 10.1021/ja407115p.
14. Jin, Y.S.; Yue, X.; Shu, C.; Huang, S.L.; Shen, P.K. Three-dimensional porous MoNi<sub>4</sub> networks constructed by nanosheets as bifunctional electrocatalysts for overall water splitting. *J. Mater. Chem. A* **2017**, *5*, 2508-2513, 10.1039/c6ta10802d.
15. McKone, J.R.; Sadtler, B.F.; Werlang, C.L.; Lewis, N.S.; Gray, H.B. Ni-Mo Nanopowders for Efficient Electrochemical Hydrogen Evolution. *ACS Catal.* **2013**, *3*, 166-169, 10.1021/cs300691m.
16. Fang, M.; Guo, W.; Dong, G.F.; Xia, Z.M.; Yip, S.P.; Qin, Y.B.; Qu, Y.Q.; Ho, J.C. Hierarchical NiMo-based 3D electrocatalysts for highly-efficient hydrogen evolution in alkaline conditions. *Nano Energy* **2016**, *27*, 247-254, 10.1016/j.nanoen.2016.07.005.
17. Jothi, P.R.; Kannan, S.; Velayutham, G. Enhanced methanol electro-oxidation over in-situ carbon and graphene supported one dimensional NiMoO<sub>4</sub> nanorods. *J. Power Sources* **2015**, *277*, 350-359, 10.1016/j.jpowsour.2014.11.137.
18. Kuang, P.Y.; Tong, T.; Fan, K.; Yu, J.G. In Situ Fabrication of Ni-Mo Bimetal Sulfide Hybrid as an Efficient Electrocatalyst for Hydrogen Evolution over a Wide pH Range. *ACS Catal.* **2017**, *7*, 6179-6187, 10.1021/acscatal.7b02225.
19. Conway, B.E.; Tilak, B.V. Interfacial processes involving electrocatalytic evolution and oxidation of H<sub>2</sub>, and the role of chemisorbed H. *Electrochim Acta* **2002**, *47*, 3571-3594, 10.1016/S0013-4686(02)00329-8.
20. Zheng, Y.; Jiao, Y.; Zhu, Y.H.; Li, L.H.; Han, Y.; Chen, Y.; Du, A.J.; Jaroniec, M.; Qiao, S.Z. Hydrogen evolution by a metal-free electrocatalyst. *Nat. Commun.* **2014**, *5*, 3783, 10.1038/ncomms4783.
21. Liang, Z.X.; Ahn, H.S.; Bard, A.J. A Study of the Mechanism of the Hydrogen Evolution Reaction on Nickel by Surface Interrogation Scanning Electrochemical Microscopy. *J. Am. Chem. Soc.* **2017**, *139*, 4854-4858, 10.1021/jacs.7b00279.